Journal of Alloys and Compounds 1010 (2025) 177389

Contents lists available at ScienceDirect

Journal of Alloys and Compounds

journal homepage: www.elsevier.com/locate/jalcom

Review

Understanding the structural and optical evolution of Eu^{3+} and Dy^{3+} co-doped YVO_4 phosphors across concentration series for lighting applications

Houssem Eddine Sekrafi [a,b,*], Eya Hergli [a,b], Stanislav Ferdov [a,b], Paulo J.G. Coutinho [a,b], Luis Rebouta [a,b]

[a] Physics Centre of Minho and Porto Universities (CF-UM-UP), University of Minho, Braga 4710-057, Portugal
[b] Laboratory of Physics for Materials and Emergent Technologies, LaPMET, University of Minho, Braga 4710-057, Portugal

ARTICLE INFO

Keywords:
Nanophosphors
White LED
Photoluminescence
YVO_4:x(Eu^{3+}, Dy^{3+}) Band gap
Energy transfer

ABSTRACT

YVO_4 nanoparticles co-doped with Eu^{3+} and Dy^{3+} ions were successfully synthesized using a conventional co-precipitation method. The resulting phosphors exhibited a single-phase trigonal YVO_4 structure, with nanoparticles averaging approximately 60 nm in size, obtained by measurements carried out with scanning electron microscope images. UV–visible diffuse reflectance spectroscopy analysis reveals that the direct band gaps of our samples fall within the range of 3.6–3.75 eV. After a thorough analysis, the optimal doping concentration was identified as 2 at% Eu^{3+} and 2 at% Dy^{3+} ions co-doping, exhibiting the strongest up-conversion emission intensity under 310 nm excitation. YVO_4:x(Eu^{3+}, Dy^{3+}) phosphors exhibit distinct bands corresponding to transitions of Dy^{3+} and Eu^{3+} ions from their $^4F_{9/2}$ and $^5D_0$ excited states, respectively. The energy transfer from Dy^{3+} to Eu^{3+} is validated through electric dipole–dipole interaction, with a critical distance of 15.63 Å. YVO_4 nanoparticles co-doped with Eu^{3+} and Dy^{3+} ions exhibit wide-range control over their photoluminescence color by regulating the concentration of both dopants. These findings suggest great potential for applications in current industrial settings.

1. Introduction

Reducing global energy consumption is a pressing challenge for researchers worldwide [1]. Developing and improving white light-emitting diodes (WLEDs) has gained significant attention as a potential replacement for conventional fluorescent and incandescent lamps [2]. This is due to WLEDs' numerous advantages, including low energy consumption, long lifespan, high luminous efficiency, and environmental friendliness [3]. WLEDs are a crucial component of modern lighting technology, with a wide range of applications in general lighting, backlighting, and automotive lighting. A common approach for achieving white light utilizes a blue LED chip coated with a yellow phosphor, known as the "blue-pumping" method [4]. However, this method suffers from limitations like low color rendering index (CRI) and high correlated color temperature (CCT) [5]. An alternative method employs a red, green, and blue (RGB) LED chip combination, enabling a wider color gamut and higher CRI [5]. However, this approach necessitates precise control over the intensity and wavelength of each LED chip, increasing complexity and cost. A promising approach utilizes a single, dual-emitting phosphor, like YVO_4:Bi^{3+}, Eu^{3+} [6,7], which simplifies manufacturing and reduces costs while maintaining high CRI and low CCT. This phosphor exhibits high thermal stability and excellent luminescence properties, making it ideal for WLED applications. Furthermore, Li^+ co-doping in the YPO_4:Dy^{3+} system presents exciting possibilities for display devices [8]. The co-doping enhances Dy^{3+} emission intensity and improves thermal stability, making the phosphor suitable for high-power WLEDs [9].

Different trivalent rare-earth (RE) ions, such as Eu^{3+}, Dy^{3+}, Tm^{3+}, and Sm^{3+}, are commonly used as activators in the vanadate host lattice [10,11]. These RE ions can also be co-doped to enhance emission efficiency through energy transfer mechanisms. However, the co-doping of divalent ions can also significantly impact the emission spectra of the material. Furthermore, yttrium vanadate (YVO_4) doped with various RE ions exhibits remarkable versatility, covering nearly the entire visible spectrum with its diverse emission colors. YVO_4 is a critical host material due to its exceptional combination of properties. These include a

* Corresponding author at: Physics Centre of Minho and Porto Universities (CF-UM-UP), University of Minho, Braga 4710-057, Portugal.
E-mail address: houssem91sek@gmail.com (H.E. Sekrafi).

https://doi.org/10.1016/j.jallcom.2024.177389
Received 4 September 2024; Received in revised form 28 October 2024; Accepted 3 November 2024
Available online 6 November 2024
0925-8388/© 2024 The Author(s). Published by Elsevier B.V. This is an open access article under the CC BY license (http://creativecommons.org/licenses/by/4.0/).

high melting point of approximately 1810 °C, isotropic light emission with a refractive index of around 2.02, low phonon energy (<900 cm^{-1}), and a direct bandgap of approximately 3.6 eV [12].

Dy^{3+} ions, with their characteristic 4 f [13] electronic configuration, exhibit emission spectra primarily originating from the $^4F_{9/2}$ energy level. This results in two distinct narrow emission lines: a blue light emission (470–500 nm) corresponding to the $^4F_{9/2} \rightarrow {}^6H_{15/2}$ transition, and a yellow light emission (570–600 nm) corresponding to the $^4F_{9/2} \rightarrow {}^6H_{13/2}$ transition [13,14]. Notably, the intensity ratio of these yellow and blue emissions is highly sensitive to the surrounding crystal environment of the Dy^{3+} ions. By carefully selecting a suitable host material and doping it solely with Dy^{3+}, white-emitting phosphors can be achieved through manipulation of this intensity ratio [15]. In contrast, Eu^{3+} ions are widely used as efficient activators for red-emitting phosphors. Their emission lines arise from electronic transitions originating from the excited $^5D_0$ level to the various ^7F_J (J = 0, 1, 2, 3, 4, 5, 6) levels within the 4 f [16,17] electronic configuration [14,18]. Importantly, the emission spectra of Eu^{3+} are strongly influenced by the symmetry of the sites they occupy within the host material. This sensitivity arises from the combined effects of electronic-dipole and magnetic-dipole interactions of the internal 4 f electrons. Therefore, the selection of an appropriate host material plays a critical role in determining the luminescent properties of inorganic phosphors by providing a suitable crystal field environment for the activator ions.

To further enhance the luminescent characteristics of YVO_4, doping with specific RE ions, such as Eu^{3+} and Dy^{3+}, presents a viable strategy. These ions introduce novel energy levels within YVO_4's band gap, resulting in heightened luminescence efficiency and customizable emission colors.

Building on this concept, researchers have investigated co-doping orthovanadates with Eu^{3+} and Dy^{3+} ions. They typically optimize the photoluminescence intensity by first doping the YVO_4 matrix with a single dopant (either Eu^{3+} or Dy^{3+}) at varying concentrations. Subsequently, they introduce a series of different concentrations of Eu or Dy into the pre-doped YVO_4:Eu^{3+} or YVO_4:Dy^{3+} matrix. Our work presents a novel approach by directly co-doping the YVO_4 matrix with equal concentrations of both Eu^{3+} and Dy^{3+} ions. The nanophosphors of YVO_4: x(Eu^{3+}, Dy^{3+}) (where x=1 at%, 2 at%, 3 at%, and 5 at%, the same x atomic concentration for both) were synthesized using a co-precipitation technique. Subsequently, a comprehensive analysis of their structural, compositional, and optical characteristics was meticulously conducted.

2. Experimental

2.1. Materials

The raw materials employed in the current study were sourced from Sigma-Aldrich (St. Louis, MO, USA), including sodium orthovanadate (Na_3VO_4) with a purity of 99.98 % (trace metals basis), yttrium nitrate hexahydrate ($Y(NO_3)_3 \bullet 6\ H_2O$) with a purity of 99.9 %, europium (III) nitrate pentahydrate ($Eu\ (NO_3)_3 \bullet 5\ H_2O$) with a purity of 99.9 %, and dysprosium (III) nitrate hydrate ($Dy\ (NO_3)_3 \bullet xH_2O$) with a purity of 99.9 % in the desired proportions.

2.2. Synthesis of YVO_4:x(Eu^{3+}, Dy^{3+}) (x = 1–5 at%) nanoparticles

The nanophosphors were prepared through co-precipitation technique [19]. One mmol of Na_3VO_4 was first dissolved in 3.5 mL of distilled water, and then, $Y(NO_3)_3 \bullet 6\ H_2O$ (1 mmol) was dissolved in 0.5 mL of distilled water. For each sample, the desired amounts of Eu $(NO_3)_3 \bullet 5\ H_2O$ and $Dy(NO_3)_3 \bullet xH_2O$ were subsequently dissolved in separate aliquots of 0.5 mL of distilled water. Different samples were prepared with Eu and Dy dopant concentrations of 1, 2, 3, and 5 at. percent (at%). The solution was stirred using a magnetic stirrer for 10 minutes at room temperature. The resulting precipitate was then centrifuged, washed with distilled water, and dried at 50 °C. Subsequently, the final product was subjected to heating in an electric muffle furnace at 800°C for a duration of 2 h. The yield of the product containing both Eu and Dy is 65 %.

2.3. Characterization

X-ray diffraction (XRD) patterns were collected using a Bruker D8 Discover diffractometer with CuKα radiation (λ = 1.5406 Å). The instrument operated in the θ/2θ scan mode over a range of 10°-70° with a step size of 0.04° and an integration time of 1 second. Energy-dispersive X-ray spectroscopy (EDS) using an EDAX Pegasus X4M analyzer, with an acceleration voltage of 15 keV, determined the chemical composition of the particles. Particle size and morphology were investigated using an FEI NOVA NanoSEM 200 scanning electron microscope (SEM). ImageJ software was employed to analyze the particle size distributions. We manually selected 100 particles from each SEM image, excluding holes, for size measurement. ImageJ can characterize both spherical and non-spherical particles using various parameters, including longest and shortest diameters, perimeter, projected area, or equivalent spherical diameter.

The reflectance of the compound was measured using a Shimadzu UV-3600i Plus UV-Vis-NIR spectrophotometer over a wavelength range of 250–850 nm with a step of 1 nm. The total reflectance was obtained with an incidence angle of 8° using a 150 mm diameter integrating sphere (model ISR-1503, Shimadzu).

A homemade portable setup equipped with a 310 nm light-emitting-diode (LED) excitation source and a CCS200 spectrometer from Thorlabs was used to measure the photoluminescence of Eu^{3+} and Dy^{3+} co-doped YVO_4 nanoparticles. All characterizations were performed at room temperature.

3. Results and discussion

3.1. XRD patterns, Phase structure and Rietveld refinement

Fig. 1.a displays X-ray diffraction (XRD) patterns of YVO_4 phosphorous with varying atomic percentages of Eu^{3+} and Dy^{3+} ions, synthesized using the co-precipitation method and subsequently thermally annealed at 800 °C. All diffraction peaks observed in the patterns can be assigned to the reference YVO_4 phase (tetragonal, space group I41/amd, JCPDS 00–016–0250). Broad and intense peaks in the X-ray diffraction pattern indicate that the nanophosphors synthesized are well-crystallized and have dimensions on the nanoscale [20]. No evidence of additional crystalline phases was found.

The Rietveld refinement analysis of YVO_4:3 % (Eu^{3+}, Dy^{3+}), chosen as the subject of analysis, was performed using the FULLPROF suite program. The Pseudo-Voigt function was utilized to fit multiple parameters of the data points [21]. Fig. 1.b illustrates the Rietveld refinement of the XRD pattern for selected nanophosphor samples with x = 3 mol%. The tetragonal structure of YVO_4 was initially used as a reference to refine the data towards the actual crystal structure. In the refinement plot, the solid line represents the calculated XRD pattern, while dots depict the observed XRD patterns. Vertical green bars indicate the Bragg positions of the tetragonal phase, and the lower profile shows the discrepancy between observed and calculated XRD patterns. The quality of the refined data was assessed by lower values of goodness of fit (GOF) = χ^2; for optimal refinement results, GOF should approach unity. Table 1 summarizes the calculated lattice parameters (a, b, c), as well as the unit cell volume (V). In the same table, we have also compiled the reliability factor (R_F), the Bragg R-factor, and the GOF. Based on the calculated values, it is evident that the refined parameters show minor deviations from the standard data for YVO_4. This observation indicates the effective and consistent integration of Europium and Dysprosium ions into the YVO_4 host matrix. This integration is made possible by the similar ionic radius and chemical reactivity shared among Eu^{3+}, Dy^{3+},

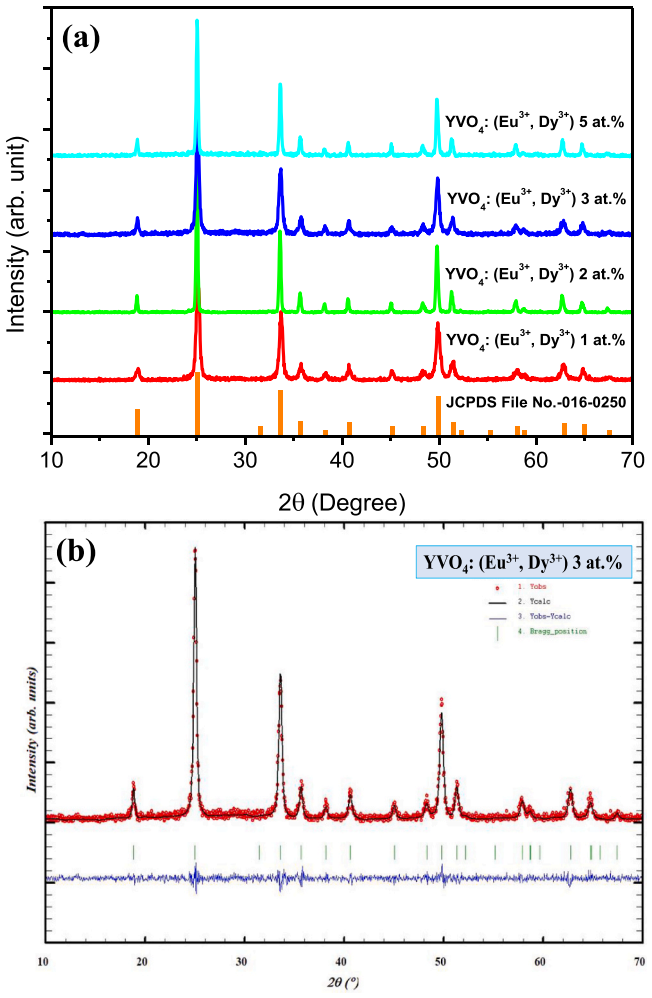

Fig. 1. (a) X-ray diffraction pattern of YVO_4:x(Eu^{3+}, Dy^{3+}) with x=1, 2, 3 and 5 mol% (b) Rietveld refinement was performed on the XRD pattern of the selected compound at a concentration of 3 mol%.

and Y^{3+} ions [22,23]. Moreover, this substitution can potentially impact the photoluminescent properties of the material, particularly the emission spectrum.

The crystallite size of the nanophosphor was determined by utilizing the most prominent diffraction peak (200) and applying Debye-Scherrer's formula as presented in Equation [24,25]:

$$D_{SC} = \frac{K\lambda}{\beta \cos\theta} \quad (1)$$

D_{SC} represents the crystallite size, where K is a constant (K ≈ 0.89), λ denotes the wavelength of the x-rays used (0.15406 nm), θ corresponds to the angle of diffraction, and β represents the full width at half maximum (FWHM in radian). The calculated values of crystallite size revealed a range of 20–36 nm, as listed in the Table 1. The FWHM of XRD diffraction peaks reflects both lattice strain and crystallite size [26]. The Williamson-Hall equation quantifies this relationship, as shown below [25,27]:

$$\beta\cos\theta = 4\varepsilon \sin\theta + \frac{K\lambda}{D_{W-H}} \quad (2)$$

By utilizing a linear regression model to analyze the curve, focusing on the relationship between 4sin (θ) (x-axis) and βcos (θ) (y-axis) as shown in Fig. 2, we successfully calculated the strain ε by identifying the slope of this graph. Simultaneously, the crystallite size $D_{W\text{-}H}$ was determined by locating the point where the curve intersects the vertical

Table 1
Refinement results and crystal structure data for the YVO_4:x(Eu^{3+}, Dy^{3+}) series (x = 1 %, 2 %, 3 %, and 5 %) were compared to the reference standard of YVO_4 (space group I41/amd, JCPDS 1–0250).

Parameters	YVO_4 PDF#16–0250	YVO_4:x(Eu^{3+}, Dy^{3+})			
	0 %	1 %	2 %	3 %	5 %
a = b (Å)	7.1230	7.116 (3)	7.1164 (12)	7.114 (3)	7.1230 (17)
c (Å)	6.2910	6.290 (3)	6.2888 (10)	6.289 (2)	6.2919 (14)
c/b	0.8832	0.8839	0.8837	0.8840	0.8833
V (Å^3)	319.19	318.51	318.48	318.31	319.24
Space group	I41/amd (141)				
Y/Eu/Dy					
X	-	0.0000	0.0000	0.0000	0.0000
Y		0.7500	0.7500	0.7500	0.7500
Z		0.1250	0.1250	0.1250	0.1250
V					
X	-	0.0000	0.0000	0.0000	0.0000
Y		0.2500	0.2500	0.2500	0.2500
Z		0.3750	0.3750	0.3750	0.3750
O					
X	-	0.0000	0.0000	0.0000	0.0000
Y		0.4360	0.4376	0.4350	0.4370
Z		0.2038	0.2045	0.1990	0.2030
R_{Bragg}	-	7.88	7.02	8.39	9.03
R_F	-	5.83	7.35	7.28	8.18
GoF	-	1.28	1.62	1.31	1.41

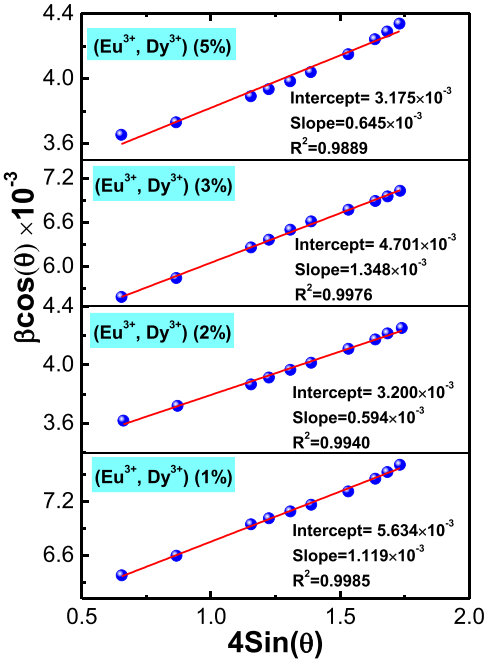

Fig. 2. W-H plot of YVO_4:x(Eu^{3+}, Dy^{3+}) nanophosphors from x=1, 2, 3 and 5 mol%.

axis at sin (θ) = 0. The obtained values are detailed in Table 2. The crystallite size estimates obtained from the Scherrer's and Williamson-Hall (W-H) plots exhibit minimal variation. This is because the strain component in Scherrer's equation is typically assumed to be negligible. However, the W-H plot reveals that the 2 % and 5 % co-doped samples of Eu^{3+} and Dy^{3+} ions exhibit relatively lower strain values and higher crystallite sizes, which is certainly correlated. In this context, it is suggested that elevated strain levels could potentially result in a reduction of fluorescence intensity [28]. The Table 2 also includes dislocation density (δ), calculated as $\delta = 1/D^2$ (D = crystallite size from

Table 2
The average crystallite size and lattice strain in the synthesized samples were estimated using Debye-Scherrer's formula and the Williamson-Hall equation.

Phosphor YVO_4:x (Eu^{3+}, Dy^{3+}) (at. mole%)	Crystallite size D (nm)		Strain ε ($\times 10^{-3}$)	Dislocation density (nm^{-2}) from Scherrer formula δ ($\times 10^{-4}$)
	D_{SC}	D_{W-H}		
1	20	25	1.12±0.02	25
2	35	43	0.59±0.01	8
3	25	30	1.35±0.02	16
5	34	44	0.65±0.03	8

Debye-Scherrer) [29]. The data reveals an inverse relationship between crystallite size, dislocation density, and strain value. This is due to the surface area effect: smaller crystallites have a higher surface area to volume ratio, leading to increased strain and dislocation density in nanomaterials [30].

3.2. Morphological analysis

The surface morphology of a luminescent material is a critical factor that significantly influences its optical properties [31]. Surface features, irregularities, and nanostructures can alter light absorption, emission efficiency, and overall optical performance. Controlling and understanding the surface morphology is essential for optimizing the optical characteristics and performance of luminescent materials across various applications. Fig. 3.a displays the SEM micrographs of as-synthetized YVO_4:x (Eu^{3+}, Dy^{3+}) (for x=1 %, 2 %, 3 %, and 5 %) nanoparticles. The SEM results reveal a porous and agglomerated morphology, consisting of polycrystalline nanoparticles. The porous structure provides a high surface area-to-volume ratio, which can be beneficial for various applications, such as catalysis, adsorption, or energy storage. The agglomeration of the nanoparticles is a common phenomenon due to the high surface energy of the nanoscale materials, leading to the formation of larger, polycrystalline structures. By comparing the SEM images, it was found that the material co-doped with 2 % Eu^{3+} and Dy^{3+} exhibits uniform and well-dispersed quasi-spherical nanoparticles. Conversely, the sample co-doped with 5 % dopants displays significantly larger grain sizes, suggesting their formation during precipitation through the fusion of smaller precursor particles. This observation aligns with previous studies, indicating that dopant concentration influences the degree of particle aggregation and size [19]. The average particle sizes observed in the SEM images (Fig. 3.b) range from 35 to 65 nm. This is larger than the corresponding crystallite sizes obtained from the XRD results, which confirms the agglomeration of the nanophosphor particles. The EDS analysis was employed to assess the chemical purity and elemental composition of the YVO_4:x(Eu^{3+}, Dy^{3+}) materials (Fig. 4). The EDX spectra confirmed the presence of Y, V, Eu, Dy, and O through the observation of their characteristic peaks. The absence of any additional peaks suggests that the prepared samples are free from significant elemental impurities.

3.3. UV-Visible reflectance spectroscopy

UV–Visible total reflectance spectra of YVO_4:x (Eu^{3+}, Dy^{3+}) doped with different concentrations of Eu^{3+} and Dy^{3+} (1, 2, 3, 5 mol%) has been depicted in Fig. 5. These measurements were carried out at ambient temperature over a wavelength range spanning from 250 nm to 850 nm. The uniform doping variation in reflectance occurs between 1 % and 5 % for the Eu^{3+} and Dy^{3+} dopants. The inset of Fig. 5 highlights the presence of a sharp absorption band at approximately 305 nm, attributed to the photoexcitation of electrons from the valence band of O^{2-} (2p electrons) to the conduction band of Y^{3+} (4d level) within the host lattice [32]. This phenomenon can be further elucidated as follows: the granular shape morphology has revealed the presence of voids in Eu^{3+} and Dy^{3+} doped YVO_4 samples. Additionally, surface defects such as Frenkel defects existing in the lattice structure contribute to absorption at various wavelengths [33]. There are also small peaks at 756 nm and 810 nm due to the f-f transition of Dy^{3+} and Eu^{3+} ions [34].

It is noteworthy that while indirect transitions may occur concurrently with direct transitions, they often go undetected in the absorption spectrum due to their high energy and low probability. The most significant transition governs the semiconductor's behavior; nevertheless, establishing the corresponding transition experimentally poses considerable challenges. The band gap energy of the co-doped YVO_4:Eu^{3+}, Dy^{3+} nanophosphors was determined by analyzing the reflectance spectra using the Kubelka-Munk (K-M or F(R)) method. The K-M function is expressed as follows [35]:

$$F(R) = \frac{(1-R)^2}{2R} \tag{3}$$

In this context, R represents the reflectance of an infinitely thick sample, while the function F(R) is directly proportional to the extinction coefficient (α). The relation given by [36] allows us to visualize the spectra based on the calculated reflectance values:

$$[F(R).h\nu]^n = A(h\nu - E_g) \tag{4}$$

In above equation, hυ denotes the energy of the incident photon, E_g stands for the energy of the optical bandgap, and A denotes a constant referred to as the band tailoring parameter. The value of 'n' varies depending on the type of transition: 2 for direct allowed transitions, 3 for direct forbidden transitions, 1/2 for indirect allowed transitions, and 3/2 for indirect forbidden transitions.

The direct band gap energy (E_{gd}) of co-doped YVO_4: Eu^{3+}, Dy^{3+} (1, 2, 3, and 5 %) was calculated by plotting the square of the K–M function $[F(R).h\nu]^2$ versus the energy in electron volts and shown in Fig. 6.**a**. The linear part of the curve was extended to $F(R)^2 = 0$ in order to determine the direct band gap energy. As shown, the band gap energy exhibits a slight increase with the concurrent co-doping of Eu and Dy, resulting in E_{gd} values of 3.6 eV, 3.65 eV, 3.69 eV, and 3.72 eV for doping levels of 1 %, 2 %, 3 %, and 5 %, respectively. The determined optical bandgap value indicates that the analyzed compound qualifies as a semiconductor material, given that E_g is lower strictly than 4 eV [37].

The observed rise in the optical band gap resulting from doping could be associated with changes in the local atomic structure or lattice configuration [38]. Another interpretation is associated with the Burstein-Moss effect (BM) [39], which clarifies the relationship between the band gap (E_g) and doping concentration. In heavily doped semiconductors, the Fermi level can shift into the conduction band (CB) due to the abundance of free charge carriers. This transition results in a notable change in the semiconductor's optical properties, leading to an apparent widening of the band gap [40].

To validate the bandgap value and its nature, Fig. 6.b shows the first derivative of reflectance ($dR/d\lambda$) for our compounds. This derivative reveals peaks at approximately 3.67 eV, 3.65 eV, 3.72 eV, and 3.76 eV, corresponding to each doping level, respectively. These peaks confirm a direct bandgap, consistent with Marotti et al. [41].

3.4. Photoluminescence

Rare earth phosphors can be broadly categorized into two types based on their emission characteristics: broad-band emission phosphors and narrow-band emission phosphors. Broad-band emission phosphors, such as those doped with Eu^{2+} or Ce^{3+}, demonstrate emission due to 5d-4f electronic transitions [42]. In contrast, narrow-band emission phosphors, such as those doped with Eu^{3+}, Gd^{3+}, Sm^{3+}, Dy^{3+}, Nd^{3+}, Tm^{3+} or Er^{3+} exhibit emission arising from 4f-4f electronic transitions [43].

Considering the 310 nm excitation wavelength used in previous work with YVO_4:Eu^{3+} 2 at% [19] and findings reported in the literature for YVO_4:Dy^{3+} 2 at% [44] phosphors, we adopted the same excitation

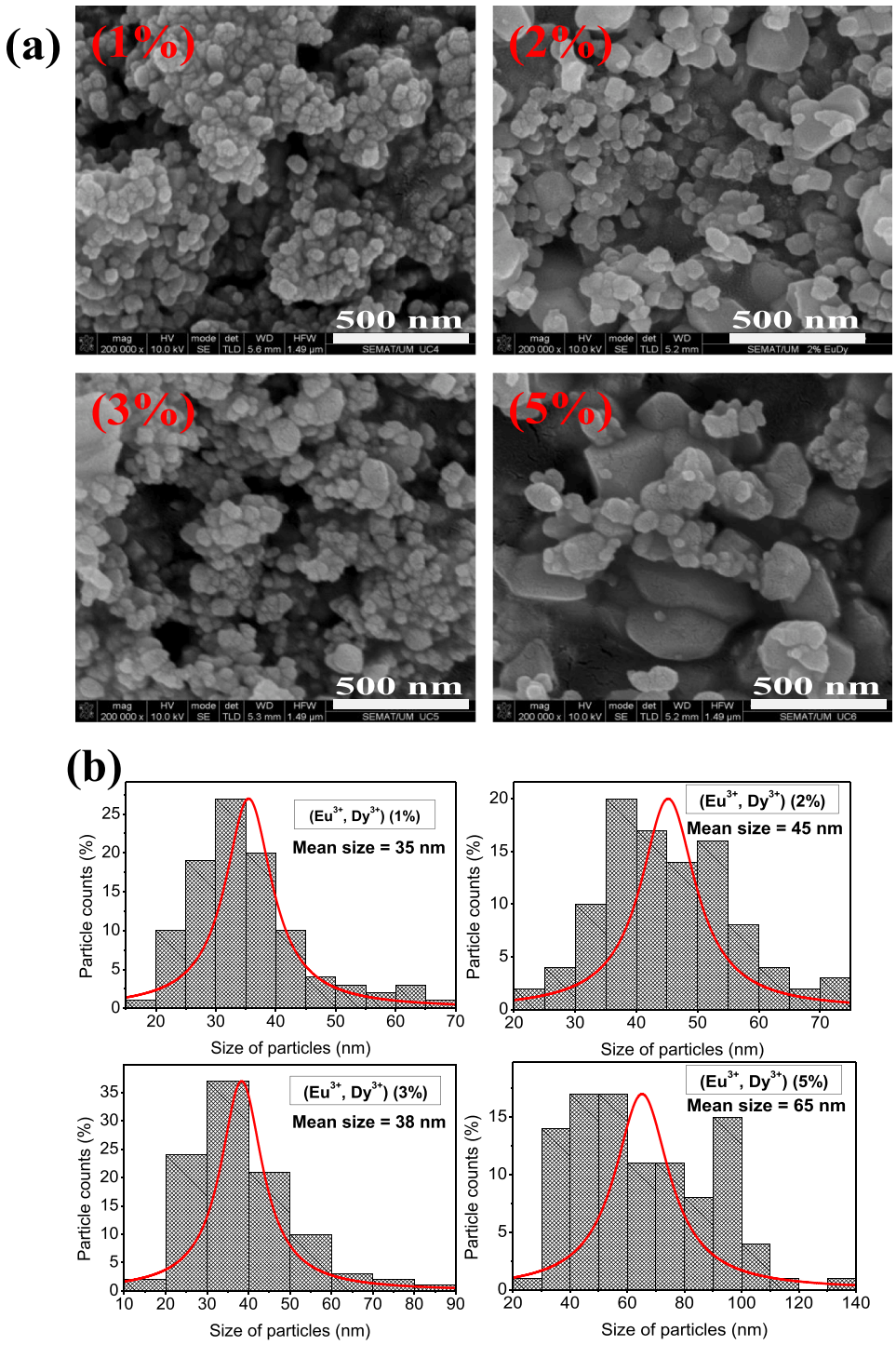

Fig. 3. (a) SEM images (b) particle distributions histogram of YVO_4:x(Eu^{3+}, Dy^{3+}) (with x=1 %, 2 %, 3 % and 5 %).

wavelength for our current investigation. Fig. 7 displays the emission spectra of the YVO_4:Ln^{3+} (Ln= Eu and/or Dy) nanocrystals, each doped with 2 at% Ln, under UV excitation. For Dy^{3+} ions, the emission peaks are centered at 486 nm ($^4F_{9/2}\rightarrow{}^6H_{15/2}$) and 577 nm ($^4F_{9/2}\rightarrow{}^6H_{13/2}$), which can produce a yellow-green light from the YVO_4:Dy^{3+} phosphors [45,46]. The intensity of the yellow emission is stronger than the green emission due to the D_{2d} point symmetry of Dy^{3+} ions without an inversion center in the YVO_4 host. The $^4F_{9/2}\rightarrow{}^6H_{13/2}$ transition is a hypersensitive forced electric dipole transition [47]. Its intensity can vary significantly by orders of magnitude depending on the local site symmetry of the emitting ion. In contrast, the intensity of the $^4F_{9/2}\rightarrow{}^6H_{15/2}$ transition is relatively insensitive to the surrounding environment [48].

The emission spectrum of YVO_4:Eu^{3+} arises from the $^5D_1\rightarrow{}^7F_1$, $^5D_1\rightarrow{}^7F_2$ and $^5D_0\rightarrow{}^7F_J$ (J = 1, 2, 3, 4) transitions of Eu^{3+} at 597 nm, 619 nm, 622 nm, 652 nm and 702 nm, which is characteristic of red phosphors [19,49]. The presence of a red peak at 619 nm and 622 nm signifies the $^5D_0\rightarrow{}^7F_2$ transition of europium ions within the YVO_4 lattice. This transition is hypersensitive, further confirming the europium ions occupy sites lacking inversion symmetry [50].

PL spectra (Fig. 7) reveal that YVO_4:2 %Dy^{3+} and YVO_4:2 %Eu^{3+} phosphors emit yellow and red light, respectively. Notably, both possess intrinsic excitation peaks in the UV–visible region. Therefore,

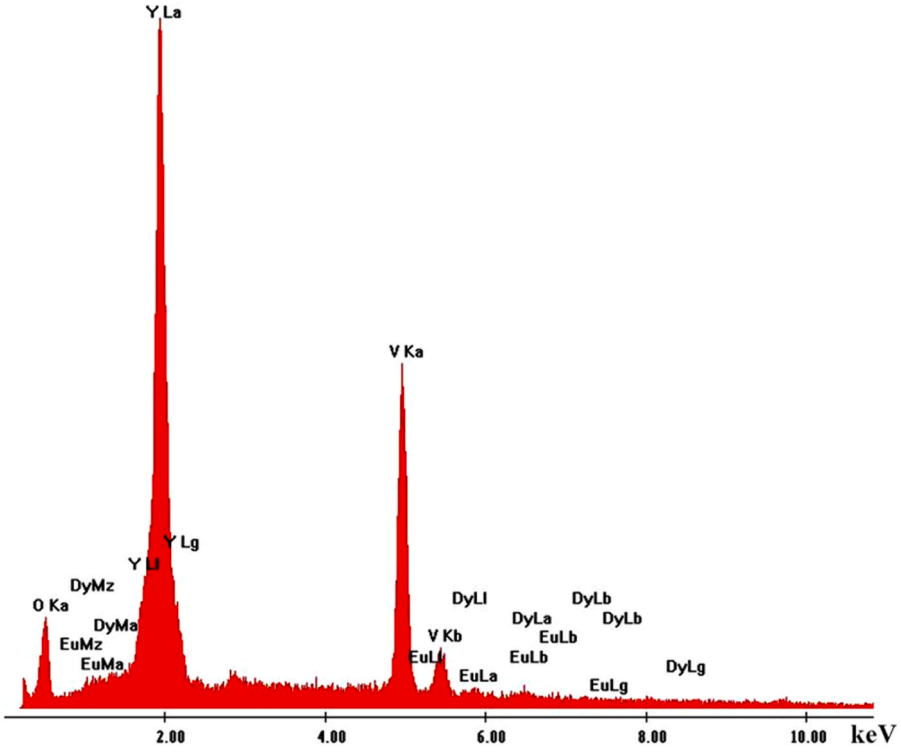

Fig. 4. The analysis of chemical elements in YVO_4 nanoparticles co-doped with Eu^{3+} and Dy^{3+} were analyzed using EDS (with x=2 % selected).

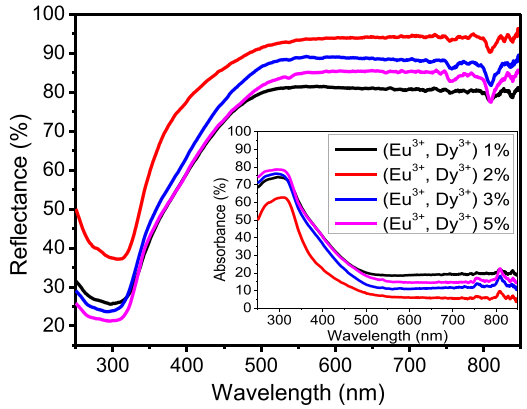

Fig. 5. Experimental UV–visible reflectance spectrum of YVO_4:x(Eu^{3+}, Dy^{3+}) (with x=1 %, 2 %, 3 % and 5 %). The inset present the absorption spectrum.

incorporating Dy^{3+} and Eu^{3+} ions simultaneously into the YVO_4 host lattice is expected to achieve tunable color in a single-phase phosphor by adjusting the activator concentration. Remarkably, the intensity of YVO_4:(Eu^{3+}, Dy^{3+}) 2 at% is higher than that of both Eu-YVO_4 and Dy-YVO_4. This observation suggests that the presence of an energy transfer mechanism between Eu^{3+} and Dy^{3+} within the YVO_4 host material, as already reported [51,52].

To investigate the effect of co-doping concentration on photoluminescence and determine the maximum allowable co-doping concentration, a series of samples were prepared with varying co-doping amounts of Eu^{3+} and Dy^{3+} (1 %, 2 %, 3 %, and 5 %), as shown in Fig. 8. The PL spectra consist of peaks at 486, 577, 597, 612, 619, 622, 655, 702, and 707 nm. There are no shifts in the peak positions of Eu^{3+} and Dy^{3+}; however, the intensity of the dopant ions increases with varying co-dopant concentrations. Inset of Fig. 8 reveals a significant enhancement in the emission intensity for YVO_4:(Eu^{3+}, Dy^{3+}) 2 at% nanophosphor compared to other co-doping concentrations. This increase in luminescence intensity might be attributed to a decrease in the strain within the crystal lattice, when compared with sample with 1 at%. In contrast, the intensity significantly decreased when the doping concentration exceeded 3 mol%. This decrease in intensity, observed with increasing concentrations of Eu^{3+} and Dy^{3+}, can be attributed to a well-known phenomenon in phosphors called concentration quenching [53,54].

The concentration quenching tends to decrease the intensity. This is due to the cross-relaxation mechanisms of Eu^{+3} and Dy^{+3}, which exhibit strong quenching behavior [55]. Energy transfer from sensitizer (Dy^{3+}) to activator (Eu^{3+}) ions in the YVO_4 matrix is a multistage interaction that typically occurs via two primary mechanisms: exchange interaction and multipolar interaction [56,57].

The exchange interactions dominate when the critical distance (R_c)is less than 5 Å, while other interactions are prominent when R_c exceeds 5 Å. According to Blasse's formula [58], the critical distance is roughly equivalent to twice the radius of a sphere that has the same volume:

$$R_C \approx 2 \left(\frac{3V}{4\pi X_c N}\right)^{1/3} \quad (5)$$

In Equation (5), V, X_C and N denote the unit cell volume, the critical concentration, and the number of lattice sites that can occupied by the activator ions, respectively. For YVO_4: Eu^{3+}, Dy^{3+} (1, 2, 3, and 5 %) phosphors, the values of these variables are known and equal to V = 319.19 $Å^3$, N = 4, and X_C = 0.04. Notably, X_C represents the total concentration of dopants required to achieve maximum energy transfer efficiency. Based on the aforementioned parameters, R_c was determined to be 15.63 Å, exceeding the effective distance of 5 Å for energy exchange interactions. Consequently, in this photoluminescent system, energy transfer occurs through the multipolar interaction mechanism, which is also the primary cause of concentration quenching. According to Dexter's energy resonance theory, the interaction type, denoted by the symbol (θ), can be expressed by the following formula [59]:

$$\frac{I}{x} = k\left(1+\beta(x)^{\theta/3}\right)^{-1} \quad (6)$$

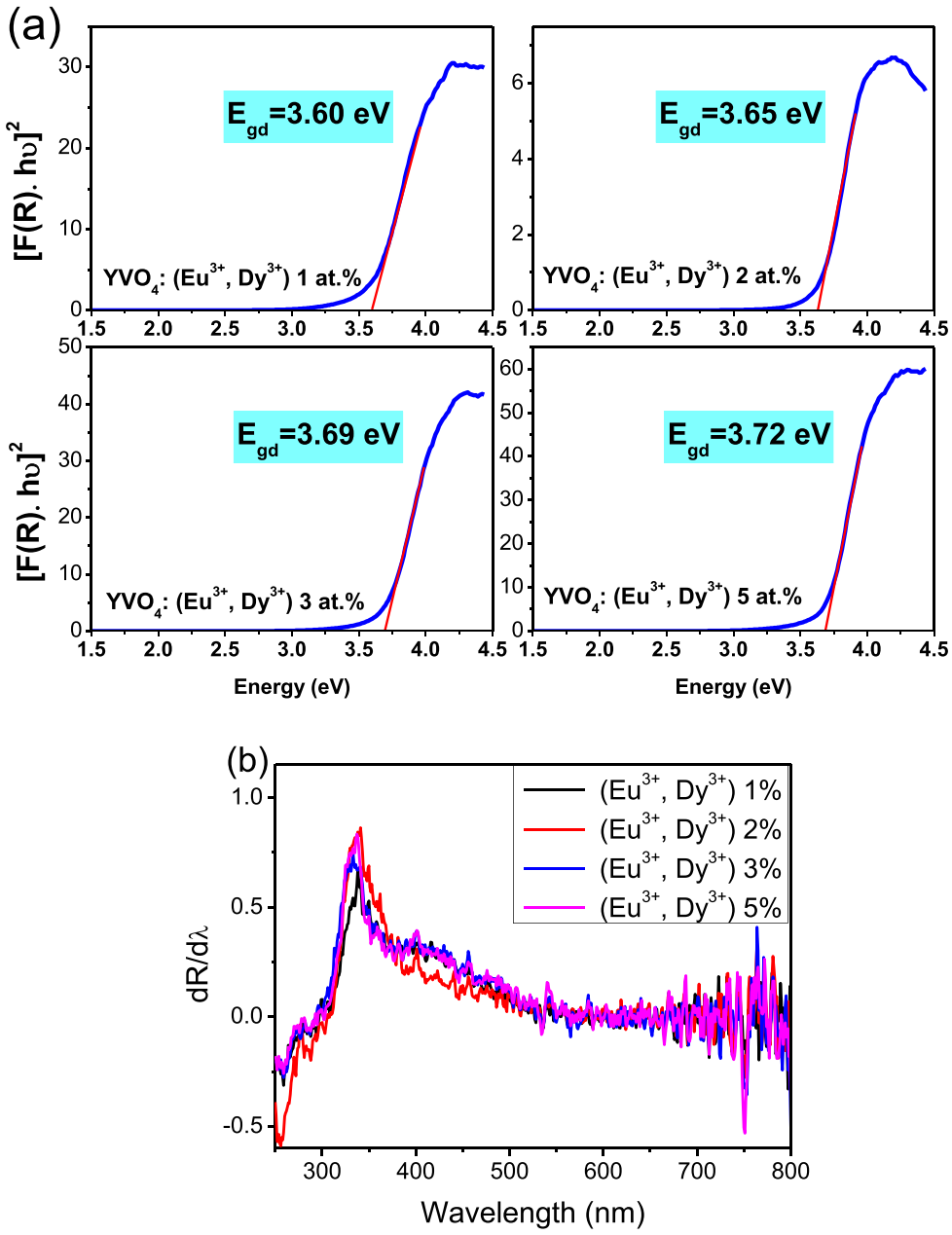

Fig. 6. Kubelka–Munk plots for of YVO_4:x(Eu^{3+}, Dy^{3+}) (with x=1 %, 2 %, 3 % and 5 %): (a) dependence of $F(R)^2$ and (b) dependence of $F(R)^{1/2}$ with gap energy. (c) Portrays the evolution of dR/dλ with wavelength.

The Eq. (6) describes the relationship between integral intensity (I), activator concentration (x), and a constant term (k). The parameter β is another constant specific to the excitation conditions of the host crystal. According to this equation, the value of θ reflects the type of energy transfer occurring. A value of θ = 3 indicates energy transfer between nearest neighbor ions. Conversely, values of θ = 6, 8, and 10 correspond to dipole-dipole (d-d), dipole-quadrupole (d-q), and quadrupole-quadrupole (q-q) interactions, respectively [60].

The multipolar character (θ) can be determined by plotting a graph of Log (I/x) versus Log (x), as shown in Fig. 9. The slope of the line, θ/3, was approximated to be −2.23 for our samples, which leads to a calculated value of θ that is approximately 6. Therefore, the concentration quenching observed in the Eu and Dy co-doped YVO_4 nanophosphor can be attributed to d-d interactions.

3.5. CIE chromaticity

The Chromaticity Coordinates (CIE, Commission International de l'Eclairage [61]) of YVO_4:x(Eu^{3+}, Dy^{3+}) phosphors were determined from the emission spectra at different x values, which are depicted in Fig. 10. The emitted light exhibits a wide color gamut, transitioning smoothly from yellow to orange and ultimately to red. This tunability suggests that the composition of YVO_4:x(Eu^{3+}, Dy^{3+}) can be precisely controlled by adjusting the x value, allowing for the targeted manipulation of the luminescent material's output color.

The quality of a light source can be often characterized by its correlated color temperature (CCT). This metric can also be determined for YVO_4:x(Eu^{3+}, Dy^{3+}) phosphors using McCamy's well-established empirical formula [62], as shown below:

$$CCT = -449n^3 + 3525n^2 - 6823n + 5520.33 \quad (7)$$

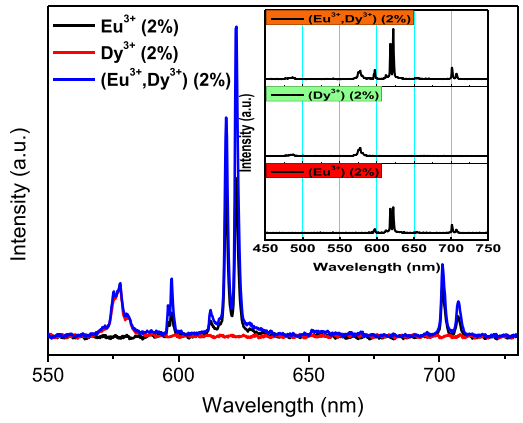

Fig. 7. Photoluminescence emission spectra of YVO_4 matrices doped with 2 % Eu^{3+} and Dy^{3+}, as well as matrices co-doped with the same concentration of both rare-earth ions.

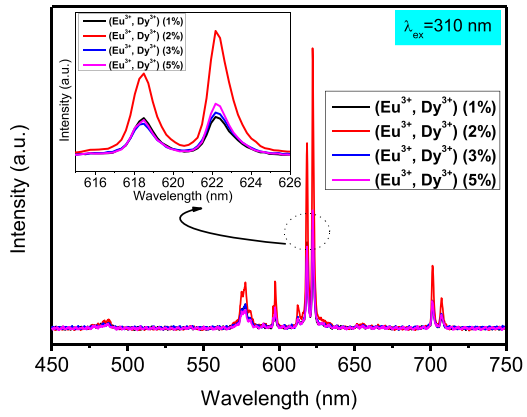

Fig. 8. Photoluminescence emission spectra of YVO_4:x(Eu^{3+}, Dy^{3+}) with x=1, 2, 3 and 5 mol% and inset show the enlarged view of highest emission intensity with a series of concentrations.

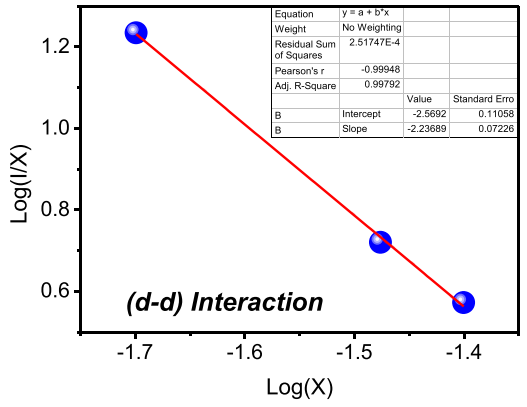

Fig. 9. Dual logarithmic graph illustrating the relationship between the photoluminescence (PL) emission intensity per co-dopant (Log(I/x)) and the concentration of Eu^{3+} and Dy^{3+} ions (Log(x)) in YVO_4:x(Eu^{3+}, Dy^{3+}) (with x=1 mol%, 2 mol%, 3 mol%, and 5 mol%) nanophosphors.

Here, $n = (x - x_e)/(x - y_e)$ represents the inverse slope of the line, with $x_e = 0.332$ and $y_e = 0.186$ denoting the coordinates of the epicenter. Table 3 presents the calculated CCT values for YVO_4:x(Eu^{3+}, Dy^{3+}) phosphors. Under 310 nm excitation, YVO_4: (Eu^{3+}, Dy^{3+}) nanophosphors co-doped with 2 % total rare earth cations display the strongest emission in the warmer orange-red spectral region, evident from their 1735 K (CCT).

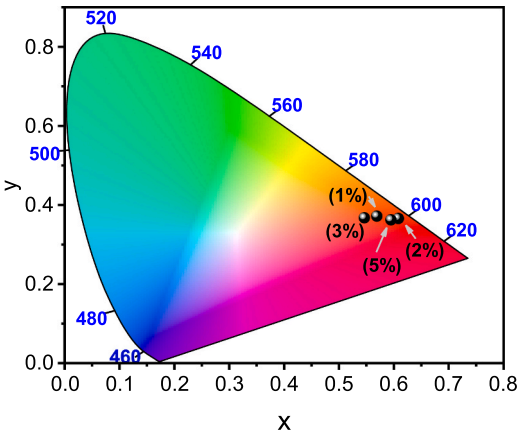

Fig. 10. CIE 1931 diagram for Eu^{3+} and Dy^{3+} co-doped YVO_4 phosphors (YVO_4:x(Eu^{3+}, Dy^{3+}) where x=1 %, 2 %, 3 %, and 5 %).

Table 3
Color chromaticity coordinates (x, y) and correlated color temperature (CCT, K) of the YVO_4:x(Eu^{3+}, Dy^{3+}) phosphors.

Compound code	Chromaticity coordinates		CCT(K)
	x	y	
YVO_4:(Eu^{3+}, Dy^{3+}) 1 %at.	0.569	0.371	1620
YVO_4:(Eu^{3+}, Dy^{3+}) 2 %at.	0.608	0.365	1735
YVO_4:(Eu^{3+}, Dy^{3+}) 3 %at.	0.546	0.367	1639
YVO_4:(Eu^{3+}, Dy^{3+}) 5 %at.	0.594	0.362	1694

YVO_4: (Eu^{3+} Dy^{3+}) nanophosphors doped with 2 % total rare earth cations exhibit the most intense emission in the warmer orange-red region of the spectrum, as evidenced by their (CCT) of 1735 K under 310 nm excitation.

4. Summary

In this study, a series of YVO_4:Eu^{3+}, Dy^{3+} samples were successfully synthesized using the co-precipitation method and then underwent thermal annealing at 800°C. XRD analysis confirmed the successful incorporation of Eu^{3+} and Dy^{3+} ions into the YVO_4 lattice without altering its tetragonal crystal structure. SEM revealed that the YVO_4: Eu^{3+}, Dy^{3+} phosphors possess a well-defined, spherically-deformed morphology with an average particle size of approximately 60 nm. This particle size range suggests promising potential for practical applications. EDX confirmed the presence of signals from yttrium, vanadium, oxygen, europium, and dysprosium, indicating also the successful doping of these ions into the YVO_4 lattice. UV–vis diffuse reflectance spectra reveal absorption peaks corresponding to an optical direct band gap in the range of 3.6–3.75 eV. In the YVO_4:x(Eu^{3+}, Dy^{3+}) phosphors, the optimal concentration of Eu^{3+} and Dy^{3+} ions for achieving the maximum up-conversion emission intensity under 310 nm excitation is 2 mol%. This concentration ratio results in the most efficient energy transfer and highest luminescence intensity. In YVO_4:x(Eu^{3+}, Dy^{3+}) phosphors, the energy transfer critical distance between Dy^{3+} and Eu^{3+} ions was calculated to be 15.63 Å. Concentration quenching in this system is attributed to dipole-dipole interactions, which dominate the energy transfer mechanism. Based on these findings, the YVO_4:(Eu^{3+}, Dy^{3+}) 2 %at. nanophosphor exhibits significant potential for use in solid-state lighting technology, particularly as a promising WLED candidate.

CRediT authorship contribution statement

Houssem Eddine Sekrafi: Writing – original draft, Software, Methodology, Investigation, Formal analysis, Data curation. **Eya Hergli:** Investigation. **Stanislav Ferdov:** Writing – review & editing, Visualization, Validation, Data curation. **Paulo J. G. Coutinho:** Writing – review & editing, Data curation. **Luis Rebouta:** Writing – review & editing, Supervision, Resources.

Declaration of Competing Interest

All authors confirm that there are no known conflicts of interest associated with this publication and that there has been no significant support for this work that could have influenced the presented results.

Acknowledgements

"This work was supported by the European Structural and Investment Funds in the FEDER Component through the Operational Competitiveness and Internationalization Programme (COMPETE 2020) under Advanced Decision Making in productive systems through Intelligent Networks (ADM.IN) Project 055087 (POCI-01–0247-FEDER-055087), and partially supported by the Portuguese Foundation for Science and Technology (FCT) in the framework of the Strategic Funding UIDB/04650/2020."

Data availability

Data will be made available on request.

References

[1] N. Bardsley, S. Bland, M. Hansen, L. Pattison, M. Pattison, K. Stober, M. Yamada, Solid-State Light. Ramp 2015 (2015), https://doi.org/10.2172/1220487 (D Plan -).
[2] H. Zhang, H. Zhang, A. Pan, B. Yang, L. He, Y. Wu, Rare earth-free luminescent materials for WLEDs: recent progress and perspectives, Adv. Mater. Technol. 6 (2021), https://doi.org/10.1002/admt.202000648.
[3] R. Mueller-Mach, G.O. Mueller, <title>White-light-emitting diodes for illumination</title>, in: H.W. Yao, I.T. Ferguson, E.F. Schubert (Eds.), 2000: pp. 30–41. https://doi.org/10.1117/12.382840.
[4] P.F. Smet, A.B. Parmentier, D. Poelman, Selecting conversion phosphors for white light-emitting diodes, J. Electrochem Soc. 158 (2011) R37, https://doi.org/10.1149/1.3568524.
[5] D. Chitnis, N. Thejo kalyani, H.C. Swart, S.J. Dhoble, Escalating opportunities in the field of lighting, Renew. Sustain. Energy Rev. 64 (2016) 727–748, https://doi.org/10.1016/j.rser.2016.06.041.
[6] J. Su, X. Mi, J. Sun, L. Yang, C. Hui, L. Lu, Z. Bai, X. Zhang, Tunable luminescence and energy transfer properties in YVO4:Bi3+, Eu3+ phosphors, J. Mater. Sci. 52 (2017) 782–792, https://doi.org/10.1007/s10853-016-0375-9.
[7] Z. Xia, D. Chen, M. Yang, T. Ying, Synthesis and luminescence properties of YVO4: Eu3+,Bi3+ phosphor with enhanced photoluminescence by Bi3+ doping, J. Phys. Chem. Solids 71 (2010) 175–180, https://doi.org/10.1016/j.jpcs.2009.10.016.
[8] A.K. Parchur, A.I. Prasad, S.B. Rai, R.S. Ningthoujam, Improvement of blue, white and NIR emissions in YPO4:Dy3+ nanoparticles on co-doping of Li+ ions, Dalton Trans. 41 (2012) 13810, https://doi.org/10.1039/c2dt32062b.
[9] A.K. Bedyal, A.K. Kunti, V. Kumar, H.C. Swart, Effects of cationic substitution on the luminescence behavior of Dy3+ doped orthophosphate phosphor, J. Alloy. Compd. 806 (2019) 1127–1137, https://doi.org/10.1016/j.jallcom.2019.07.305.
[10] J. Shao, C. Liu, X. Zhou, L. Hong, J. Yan, Z. Kang, Luminescence properties of YVO4: Ln (Ln = Dy3+, Eu3+, Tm3+) for white LED by hydrothermal method, Mater. Sci. Semicond. Process 84 (2018) 58–63, https://doi.org/10.1016/j.mssp.2018.04.007.
[11] O. Tegus, B. Amurisana, S. Zhiqiang, Morphology-sensitive photoluminescent properties of YVO4:Ln3+ (Ln3+ = Eu3+, Sm3+, Dy3+, Tm3+) hierarchitectures, J. Lumin 215 (2019) 116624, https://doi.org/10.1016/j.jlumin.2019.116624.
[12] P. Kumari, P.K. Baitha, J. Manam, Structural and photoluminescence properties of red-light emitting YVO4:Eu3+ phosphor synthesized by combustion and solid-state reaction techniques: a comparative study, Indian J. Phys. 89 (2015) 1297–1306, https://doi.org/10.1007/s12648-015-0712-x.
[13] G.M. Cai, N. Yang, H.X. Liu, J.Y. Si, Y.Q. Zhang, Single-phased and color tunable LiSrBO 3:Dy 3+, Tm 3+, Eu 3+ phosphors for white-light-emitting application, J. Lumin 187 (2017) 211–220, https://doi.org/10.1016/j.jlumin.2017.03.017.
[14] B.C. Grabmaier, Luminescent materials for medical application, J. Lumin 60–61 (1994) 967–970, https://doi.org/10.1016/0022-2313(94)90322-0.
[15] Q. Su, Z. Pei, L. Chi, H. Zhang, Z. Zhang, F. Zou, The yellow-to-blue intensity ratio (Y/B) of Dy3+ emission, J. Alloy. Compd. 192 (1993) 25–27, https://doi.org/10.1016/0925-8388(93)90174-L.
[16] Z. Wang, Q. Zhu, X. Wang, X. Li, X. Sun, B.-N. Kim, J.-G. Li, Multi-color luminescent m-LaPO $_4$:Ce/Tb monospheres of high efficiency via topotactic phase transition and elucidation of energy interaction, Inorg. Chem. 58 (2019) 890–899, https://doi.org/10.1021/acs.inorgchem.8b03029.
[17] Y. Shi, J. Ye, Y. Qi, M.A. Akram, A. Rauf, G. Ning, An anionic layered europium(<scp>iii</scp>) coordination polymer for solvent-dependent selective luminescence sensing of Fe 3+ and Cu 2+ ions and latent fingerprint detection, Dalton Trans. 47 (2018) 17479–17485, https://doi.org/10.1039/C8DT04042G.
[18] P.A. Tanner, Some misconceptions concerning the electronic spectra of tri-positive europium and cerium, Chem. Soc. Rev. 42 (2013) 5090, https://doi.org/10.1039/c3cs60033e.
[19] H.E. Sekrafi, E. Hergli, S. Ferdov, A. Mota, J. Lopes, P.J.G. Coutinho, L. Rebouta, Optimization of photoluminescence of Eu3+ doped YVO4 nanoparticles by green microwave synthesis, Mater. Chem. Phys. 312 (2024) 128592, https://doi.org/10.1016/j.matchemphys.2023.128592.
[20] T.S. Sreena, P.P. Rao, A.K.V. Raj, T.R.A. Thara, Narrow-band red-emitting phosphor, Gd 3 Zn 2 Nb 3 O 14:Eu 3+ with high color purity for phosphor-converted white light emitting diodes, J. Alloy. Compd. 751 (2018) 148–158, https://doi.org/10.1016/j.jallcom.2018.04.135.
[21] A. Dwivedi, M. Srivastava, A. Dwivedi, A. Srivastava, A. Mishra, S.K. Srivastava, Synthesis and enhanced photoluminescence properties of red emitting divalent ion (Ca2+) doped Eu:Y2O3 nanophosphors for optoelectronic applications, J. Rare Earths 40 (2022) 1187–1198, https://doi.org/10.1016/j.jre.2021.11.001.
[22] L. Zhu, J. Li, Q. Li, X. Liu, J. Meng, X. Cao, Sonochemical synthesis and photoluminescent property of YVO $_4$:Eu nanocrystals, Nanotechnology 18 (2007) 055604, https://doi.org/10.1088/0957-4484/18/5/055604.
[23] I.E. Kolesnikov, A.A. Kalinichev, M.A. Kurochkin, E.V. Golyeva, A.S. Terentyeva, E. Yu Kolesnikov, E. Lähderanta, Structural, luminescence and thermometric properties of nanocrystalline YVO4:Dy3+ temperature and concentration series, Sci. Rep. 9 (2019) 2043, https://doi.org/10.1038/s41598-019-38774-6.
[24] R. Yantake, M. Kaiheriman, T. Yusufu, A. Sidike, Effect of Li+ doping on the luminescence performance of a novel KAlSiO4:Tb3+ green-emitting phosphor, Sci. Rep. 11 (2021) 5123, https://doi.org/10.1038/s41598-021-84220-x.
[25] K. Guettiti, H.E. Sekrafi, S. Azizi, C. Bouzidi, N. Bouguila, K. Khirouni, J. Lamloumi, The study of structural, dielectric, impedance and modulus properties of La0·8Pb0·2FeO3 doped by 25% Mg into the B-site, Phys. B Condens Matter 655 (2023) 414771, https://doi.org/10.1016/j.physb.2023.414771.
[26] H.E. Sekrafi, A. Ben Jazia Kharrat, M.A. Wederni, K. Khirouni, N. Chniba-Boudjada, W. Boujelben, Structural, electrical, dielectric properties and conduction mechanism of sol-gel prepared Pr0.75Bi0.05Sr0.1Ba0.1Mn0.98Ti0.02O3 compound, Mater. Res Bull. 111 (2019) 329–337, https://doi.org/10.1016/j.materresbull.2018.11.041.
[27] P. Kumari, J. Manam, Enhanced red emission on co-doping of divalent ions (M2+= Ca2+, Sr2+, Ba2+) in YVO4:Eu3+ phosphor and spectroscopic analysis for its application in display devices, Spectrochim. Acta A Mol. Biomol. Spectrosc. 152 (2016) 109–118, https://doi.org/10.1016/j.saa.2015.07.039.
[28] A. Dwivedi, M. Srivastava, A. Srivastava, C. Upadhyay, S.K. Srivastava, Tunable photoluminescence and energy transfer of Eu3+,Ho3+-doped Ca0.05Y1.93-xO2 nanophosphors for warm white LEDs applications, Sci. Rep. 12 (2022) 5824, https://doi.org/10.1038/s41598-022-09630-x.
[29] J.B. Prasanna kumar, G. Ramgopal, Y.S. Vidya, K.S. Anantharaju, B. Daruka Prasad, S.C. Sharma, S.C. Prashantha, H.B. Premkumar, H. Nagabhushana, Bio-inspired synthesis of Y2O3: Eu3+ red nanophosphor for eco-friendly photocatalysis, Spectrochim. Acta A Mol. Biomol. Spectrosc. 141 (2015) 149–160, https://doi.org/10.1016/j.saa.2015.01.055.
[30] H.J. Rajendra, C. Pandurangappa, Synthesis and luminescence properties of europium-codoped and dysorium-doped YVO4 nanophosphor for potential applications, Appl. Phys. A 125 (2019) 702, https://doi.org/10.1007/s00339-019-2990-1.
[31] G. Jia, C. Zhang, S. Ding, L. Wang, L. Li, H. You, Synthesis and enhanced luminescence of uniform and well-dispersed quasispherical YVO $_4$:Ln $^{3+}$ (Ln = Eu, Dy) nanoparticles by a solvothermal method, CrystEngComm 14 (2012) 573–578, https://doi.org/10.1039/C1CE05725A.
[32] A. Dwivedi, M. Srivastava, A. Srivastava, C. Upadhyay, S.K. Srivastava, Tunable photoluminescence and energy transfer of Eu3+,Ho3+-doped Ca0.05Y1.93-xO2 nanophosphors for warm white LEDs applications, Sci. Rep. 12 (2022) 5824, https://doi.org/10.1038/s41598-022-09630-x.
[33] C. Pandurangappa, B.N. Lakshminarasappa, B.M. Nagabhushana, Synthesis and characterization of CaF2 nanocrystals, J. Alloy. Compd. 489 (2010) 592–595, https://doi.org/10.1016/j.jallcom.2009.09.118.
[34] H.J. Rajendra, C. Pandurangappa, D.L. Monika, Luminescence properties of dysprosium doped YVO4 phosphor, J. Rare Earths 36 (2018) 1245–1249, https://doi.org/10.1016/j.jre.2018.07.001.
[35] R. Muhammad, M.A. Khalil, M.S. Castro, Structure and dielectric characteristics of Ba1-Ca Ti1-Ca O3-δ ceramics, Ceram. Int 46 (2020) 1059–1064, https://doi.org/10.1016/j.ceramint.2019.09.072.
[36] M. Arshad, W. Khan, M. Abushad, M. Nadeem, S. Husain, A. Ansari, V. K. Chakradhary, Correlation between structure, dielectric and multiferroic properties of lead free Ni modified BaTiO3 solid solution, Ceram. Int 46 (2020) 27336–27351, https://doi.org/10.1016/j.ceramint.2020.07.219.
[37] O. Ben Moussa, H. Chebbi, M.F. Zid, Synthesis, crystal structure, vibrational study, optical properties and Hirshfeld surface analysis of bis(2,6-diaminopyridinium)

tetrachloridocobaltate(II) monohydrate, J. Mol. Struct. 1180 (2019) 72–80, https://doi.org/10.1016/j.molstruc.2018.11.077.
[38] M.L.A. Letswalo, L. Reddy, A. Balakrishna, H.C. Swart, O.M. Ntwaeaborwa, Influence of SO42− anionic group substitution on the enhanced photoluminescence behaviour of red emitting CaMoO4:Eu3+ phosphor, J. Alloy. Compd. 854 (2021) 157022, https://doi.org/10.1016/j.jallcom.2020.157022.
[39] Y.H. Yang, X.Y. Chen, Y. Feng, G.W. Yang, Physical Mechanism of Blue-Shift of UV Luminescence of a Single Pencil-Like ZnO Nanowire, Nano Lett. 7 (2007) 3879–3883, https://doi.org/10.1021/nl071849h.
[40] V. Ivchenko, Theory of Burstein-Moss effect in semiconductors with anisotropic energy bands, Phys. Scr. 99 (2024) 035952, https://doi.org/10.1088/1402-4896/ad28e5.
[41] R. Mguedla, A. Ben Jazia Kharrat, M. Saadi, K. Khirouni, N. Chniba-Boudjada, W. Boujelben, Structural, electrical, dielectric and optical properties of PrCrO3 ortho-chromite, J. Alloy. Compd. 812 (2020) 152130, https://doi.org/10.1016/j.jallcom.2019.152130.
[42] X. Qin, X. Liu, W. Huang, M. Bettinelli, X. Liu, Lanthanide-activated phosphors based on 4f-5d optical transitions: theoretical and experimental aspects, Chem. Rev. 117 (2017) 4488–4527, https://doi.org/10.1021/acs.chemrev.6b00691.
[43] X. Xu, J. Zhao, H. Feng, Z. Gao, L. Guan, Y. Yang, F. Wang, D. Wang, X. Li, Preparation, luminescence properties and electronic structure of RE (RE=Eu3+, Sm3+,Dy3+)-doped multi-color silico-phosphate Ca15(PO4)2(SiO4)6 phosphors, J. Lumin 226 (2020) 117356, https://doi.org/10.1016/j.jlumin.2020.117356.
[44] I.E. Kolesnikov, A.A. Kalinichev, M.A. Kurochkin, E.V. Golyeva, A.S. Terentyeva, E. E.Yu. Kolesnikov, Lähderanta, Structural, luminescence and thermometric properties of nanocrystalline YVO4:Dy3+ temperature and concentration series, Sci. Rep. 9 (2019) 2043, https://doi.org/10.1038/s41598-019-38774-6.
[45] M. Yu, J. Lin, Z. Wang, J. Fu, S. Wang, H.J. Zhang, Y.C. Han, Fabrication, Patterning, and Optical Properties of Nanocrystalline YVO $_4$:A (A = Eu $^{3+}$, Dy $^{3+}$, Sm $^{3+}$, Er $^{3+}$) Phosphor Films via Sol−Gel Soft Lithography, Chem. Mater. 14 (2002) 2224–2231, https://doi.org/10.1021/cm011663y.
[46] J. Shao, C. Liu, X. Zhou, L. Hong, J. Yan, Z. Kang, Luminescence properties of YVO4: Ln (Ln = Dy3+, Eu3+, Tm3+) for white LED by hydrothermal method, Mater. Sci. Semicond. Process 84 (2018) 58–63, https://doi.org/10.1016/j.mssp.2018.04.007.
[47] J. Kuang, Y. Liu, J. Zhang, White-light-emitting long-lasting phosphorescence in Dy3+-doped SrSiO3, J. Solid State Chem. 179 (2006) 266–269, https://doi.org/10.1016/j.jssc.2005.10.025.
[48] P. Babu, K.H. Jang, E.S. Kim, L. Shi, H.J. Seo, F. Rivera-López, U.R. Rodríguez-Mendoza, V. Lavín, R. Vijaya, C.K. Jayasankar, L. Rama Moorthy, Spectral investigations on Dy3+-doped transparent oxyfluoride glasses and nanocrystalline glass ceramics, J. Appl. Phys. 105 (2009), https://doi.org/10.1063/1.3021451.
[49] L. Li, M. Zhao, W. Tong, X. Guan, G. Li, L. Yang, Preparation of cereal-like Y V O $_4$: Ln $^{3+}$ (Ln = Sm, Eu, Tb, Dy) for high quantum efficiency photoluminescence, Nanotechnology 21 (2010) 195601, https://doi.org/10.1088/0957-4484/21/19/195601.
[50] W. Wang, Z. Cheng, P. Yang, Z. Hou, C. Li, G. Li, Y. Dai, J. Lin, Patterning of YVO $_4$: Eu $^{3+}$ luminescent films by soft lithography, Adv. Funct. Mater. 21 (2011) 456–463, https://doi.org/10.1002/adfm.201001467.
[51] H.J. Rajendra, C. Pandurangappa, Cathodoluminescence Studies of Europium, Dysprosium and Eu, Dy Co-doped YVO4 Nanophosphor, J. Inst. Eng. (India): Ser. E 104 (2023) 19–27, https://doi.org/10.1007/s40034-022-00260-6.
[52] J. Shao, C. Liu, X. Zhou, L. Hong, J. Yan, Z. Kang, Luminescence properties of YVO4: Ln (Ln = Dy3+, Eu3+, Tm3+) for white LED by hydrothermal method, Mater. Sci. Semicond. Process 84 (2018) 58–63, https://doi.org/10.1016/j.mssp.2018.04.007.
[53] D.L. Dexter, J.H. Schulman, Theory of Concentration Quenching in Inorganic Phosphors, J. Chem. Phys. 22 (1954) 1063–1070, https://doi.org/10.1063/1.1740265.
[54] R.F. Bogale, Y. Chen, J. Ye, Y. Yang, A. Rauf, L. Duan, P. Tian, G. Ning, Highly selective and sensitive detection of 4-nitrophenol and Fe3+ ion based on a luminescent layered terbium (III) coordination polymer, Sens Actuators B Chem. 245 (2017) 171–178, https://doi.org/10.1016/j.snb.2017.01.177.
[55] H.J. Rajendra, C. Pandurangappa, Synthesis and luminescence properties of europium-codoped and dysorium-doped YVO4 nanophosphor for potential applications, Appl. Phys. A 125 (2019) 702, https://doi.org/10.1007/s00339-019-2990-1.
[56] B. Devakumar, P. Halappa, C. Shivakumara, Dy3+/Eu3+ co-doped CsGd(MoO4)2 phosphor with tunable photoluminescence properties for near-UV WLEDs applications, Dyes Pigments 137 (2017) 244–255, https://doi.org/10.1016/j.dyepig.2016.10.016.
[57] R. Vijayakumar, H. Guo, X. Huang, Energy transfer and color-tunable luminescence properties of Dy3+ and Eu3+ co-doped Na3Sc2(PO4)3 phosphors for near-UV LED-based warm white LEDs, Dyes Pigments 156 (2018) 8–16, https://doi.org/10.1016/j.dyepig.2018.03.053.
[58] G. Blasse, Energy transfer in oxidic phosphors, Phys. Lett. A 28 (1968) 444–445, https://doi.org/10.1016/0375-9601(68)90486-6.
[59] J. Tang, J. Si, X. Fan, Y. Liu, G. Li, G. Cai, Tunable emission, energy transfer and thermal stability of Ce3+, Tb3+ co-doped Na2BaCa(PO4)2 phosphors, J. Rare Earths 40 (2022) 878–887, https://doi.org/10.1016/j.jre.2021.05.016.
[60] M. Xia, S. Gu, C. Zhou, L. Liu, Y. Zhong, Y. Zhang, Z. Zhou, Enhanced photoluminescence and energy transfer performance of Y $_3$ Al $_4$ GaO $_{12}$:Mn $^{4+}$,Dy $^{3+}$ phosphors for plant growth LED lights, RSC Adv. 9 (2019) 9244–9252, https://doi.org/10.1039/C9RA00700H.
[61] Y. Guo, B.K. Moon, B.C. Choi, J.H. Jeong, J.H. Kim, Color–tunable luminescence and energy transfer behaviors of Dy3+/Eu3+ co–doped SrLaMgTaO6 phosphors for solid state lighting applications, Mater. Res Bull. 88 (2017) 166–173, https://doi.org/10.1016/j.materresbull.2016.12.035.
[62] C.S. McCamy, Correlated color temperature as an explicit function of chromaticity coordinates, Color Res Appl. 17 (1992) 142–144, https://doi.org/10.1002/col.5080170211.